

# Gradient Aware Cascade Network for Multi-Focus Image Fusion

Boyuan Ma, <sup>\*1,2,3</sup> Xiang Yin, <sup>\*1,2,3</sup> Di Wu, <sup>4</sup> Xiaojuan Ban, <sup>†1,2,3</sup> Haiyou Huang, <sup>‡1,5</sup>

<sup>1</sup>Beijing Advanced Innovation Center for Materials Genome Engineering, University of Science and Technology Beijing, China.

<sup>2</sup>School of Computer and Communication Engineering, University of Science and Technology Beijing, China.

<sup>3</sup>Beijing Key Laboratory of Knowledge Engineering for Materials Science, Beijing, China.

<sup>4</sup>Department of ICT and Natural Sciences, Norwegian University of Science and Technology, Aalesund, Norway.

<sup>5</sup>Institute for Advanced Materials and Technology, University of Science and Technology Beijing, China.

## Abstract

The general aim of multi-focus image fusion is to gather focused regions of different images to generate a unique all-in-focus fused image. Deep learning based methods become the mainstream of image fusion by virtue of its powerful feature representation ability. However, most of the existing deep learning structures failed to balance fusion quality and end-to-end implementation convenience. End-to-end decoder design often leads to poor performance because of its non-linear mapping mechanism. On the other hand, generating an intermediate decision map achieves better quality for the fused image, but relies on the rectification with empirical post-processing parameter choices. In this work, to handle the requirements of both output image quality and comprehensive simplicity of structure implementation, we propose a cascade network to simultaneously generate decision map and fused result with an end-to-end training procedure. It avoids the dependence on empirical post-processing methods in the inference stage. To improve the fusion quality, we introduce a gradient aware loss function to preserve gradient information in output fused image. In addition, we design a decision calibration strategy to decrease the time consumption in the application of multiple image fusion. Extensive experiments are conducted to compare with 16 different state-of-the-art multi-focus image fusion structures with 6 assessment metrics. The results prove that our designed structure can generally ameliorate the output fused image quality, while implementation efficiency increases over 30% for multiple image fusion.

## Introduction

Multi-focus image fusion is an important topic in image processing. The limitation of optical lenses naturally presents that only objects within the depth-of-field (DOF) have a focused and clear appearance in a photograph, while other objects are likely to be blurred. Hence it is difficult for objects at varying distances to all be in focus in one camera shot (Li et al. 2017). Many algorithms have been designed to create an all-in-focus image by fusing multiple source images that capture the same scene with different focus points. The fused image can be used for visualization and further processing, such as object recognition and segmentation.

Deep learning based solutions (Yann, Yoshua, and Geoffrey 2015) are accepted to be the prevailing choice for image fusion by virtue of its powerful feature representation ability. (Liu et al. 2017) introduced a convolution neural network (CNN) to image fusion and proposed a CNN-Fuse fusion method to recognize which part of the image is in-focus with a supervised deep learning structure. CNN-Fuse reached a better performance compared to traditional fusion algorithms based on the handcrafted features. (Ma et al. 2019) moved further in applying an unsupervised training strategy to fuse images, termed as SESF-Fuse. It avoided heavy labeling work for images to train the network.

Although deep learning has reached relatively good performance in multi-focus image fusion, the new problems yielded with complex structure design remain unsolved. There are three questions that deserve higher priorities. 1) The balance between fusion quality and end-to-end implementation convenience. Some structures tried to use a decoder to directly output the final fused result (Huang et al. 2020; Zhang et al. 2020a). However, they did not preserve true pixel values in the source image and hardly achieve good performance in fusing evaluation due to the non-linear mapping mechanism in the decoder. Some other structures generated intermediate decision map (DM) to reconstruct fused result with high quality (Liu et al. 2017; Xu et al. 2020a). But they relied highly on post-processing method (or consistency verification) choices. These methods require empirical parameters to rectify the DM, resulting in limits the generalization of them to different scenes of image fusion. 2) The gradient feature contains rich beneficial information for multi-focus image fusion. However, it was overlooked in many designs. Some deep learning structures used the l2 and SSIM objective functions to optimize the network (Li and Wu 2019; Ram, Sai, and Venkatesh 2017). These made the gradient feature completely lost during training procedure. 3) The efficiency in multiple image fusion. Currently, most of the multi-focus fusion structures focus on two image fusion task. With multiple image fusion, the strategy is to go one by one in serial sequence (Ma et al. 2019). However, the results in time consumption is scarcely acceptable for big volume image fusions.

In order to counterpoise the requirements of fused image quality and training simplicity, we design a gradient aware

\* indicates equal contribution.

† corresponding authors: banxj@ustb.edu.cn.

‡ corresponding authors: huanghy@mater.ustb.edu.cn.

cascade structure, termed GACN<sup>1</sup>. It simultaneously generates decision map and fused result with an end-to-end training procedure. The original pixel values in the source are retained to optimize output fused image bypassing empirical post-processing methods. Furthermore, we modify a commonly used gradient based evaluation metric as the training loss function in order to preserve gradient information. For multiple image fusion, we simplify redundant calculations by proposing a calibration module to acquire the activity levels of all images. It helps to significantly decrease the time consumption. We highlight our contributions as follows:

- We propose a network to simultaneously generate decision map and fused result with an end-to-end training procedure.
- We introduce a gradient aware loss function to preserve gradient information and improve output fusion quality.
- We design a decision calibration strategy for multiple image fusion in order to increase implementation efficiency.
- To prove the feasibility and efficiency of the proposed GACN, we conduct extensive experiments to compare with 16 different state-of-the-art (SOTA) multi-focus image fusion structures with 6 assessment metrics. We implement overall ablation studies additionally to test the impact of different modules in our structure. The results prove that our designed structure can generally ameliorate the output fused image quality, and increase implementation efficiency over 30% for multiple image fusion.

## Related Work

The existing solutions for multi-focus image fusion can be generalized into two orientations: handcrafted feature based and deep learning based algorithms.

### Handcrafted Feature Based Fusion Algorithms

Handcrafted feature based fusion algorithms concentrate on the profound image analysis of transform or spatial domains. Transform domain based algorithms adopt decomposed coefficients from a selected transform domain to measure different activity levels in the input source images, such as laplacian pyramid (LP) (Burt and Adelson 1983) and non-subsampled contourlet transform (NSCT) (Zhang and long Guo 2009). Spatial domain based algorithms measure activity levels with gradient features, such as spatial frequency (Li, Kwok, and Wang 2001), multi-scale weighted gradient (MWG) (Zhou, Li, and Wang 2014), and dense SIFT (DSIFT) (Liu, Liu, and Wang 2015).

### Deep Learning Based Fusion Algorithms

Deep learning based algorithms provide prevalent solutions to image fusion problems. CNN-Fuse (Liu et al. 2017) first used a convolutional network to automatically learn features in each patch of image and decided which patch is the clarity region, which achieved better performance compared to

handcrafted feature based algorithms. Afterward, some researchers tried to modify the network to improve the fusion quality or efficiency. (Tang et al. 2017) proposed a pixel-wise fusion CNN to further improve the fusion quality. Dense-Fuse (Li and Wu 2019), U2Fusion (Xu et al. 2020b), and SESF-Fuse (Ma et al. 2019) fused images in the unsupervised training procedure, which is suited to practical application. IFCNN (Zhang et al. 2020b) presented a general image fusion framework to handle different kinds of image fusion tasks. However, there are still other parts of deep learning based algorithm that need to refine.

The output mode is an important module in network designing. Some algorithms tried to use a decoder to directly output the fused result. PMGI (Zhang et al. 2020a) used only one convolutional layer in decoder to fuse multi-scale features and generate fused result. To improve the reconstructive ability, (H et al. 2020) used residual block to improve the efficiency of gradient propagation, and (Huang et al. 2020; Zhang et al. 2021) used generative adversarial network to automatically ameliorate fusion quality. However, due to nonlinear mapping in the decoder, these structures cannot precisely reconstruct fused result. This leads to relatively poor performance in fusion evaluation. Therefore, some structures resorted to generate an intermediate DM, to decide which pixel should appear in fused result. (Liu et al. 2017; Li et al. 2020) used CNN to directly output DM. (Ma et al. 2019) used spatial frequency to calculate gradient in deep features and draw out DM. (Xu et al. 2020a) used a binary gradient relation map to further ask decoder to preserve gradient information in DM. Despite the highly fusing quality of these structures, they need some post-processing methods (or consistency verification) with empirical parameters to rectify the DM, such as morphology operations (opening and closing calculation) and small region removal strategy, which limits the generalization of the structure to different scenes of image fusion.

The objective function is a key point in structure's optimization. In the field of multi-focus image fusion, the gradient in source images is an important factor to decide which part of the image is clear. However, many deep learning structures only used the l2 norm and SSIM objective function to optimize the network (Li and Wu 2019; Ram, Sai, and Venkatesh 2017), which did not ask the network to preserve the gradient information in fused image. (H et al. 2020) proposed structure tensor to preserve the overall contrast of images. (Li et al. 2020) used an edge-preserving loss function to preserve gradient information, but it only considered gradient intensity and not took orientation information into account. In this work, we try to modify the commonly used classical gradient based evaluation metric as the loss function to directly optimize the network to export clearly fused result.

The most applications of multi-focus fusion are based on multiple images. However, almost multi-focus fusion structures concentrated on two images scene and only used one by one serial fusion strategy for multiple images (Liu et al. 2017; Xu et al. 2020b), which has in-acceptable time consumption. To the best of our knowledge, we are the first work to concentrate on the implementation efficiency in multiple

<sup>1</sup>The code and data are available at <https://github.com/Keep-Passion/GACN>.

image fusion scene.

## Method

In this section, we illustrate the details of the main contributions of this work, such as the network structure, the loss function, and the decision calibration strategy.

### Network Structure

The overall fusion network structure is shown in Figure 1. It includes two paths of convolutional operations, feature extraction and decision. First, we use the feature extraction path to collect multi-scale deep features of each source image. Second, we take spatial frequency (SF) module to calculate activity level of each scale. Third, in the decision path, we concatenate multi-scale activity levels and feed them into some convolutional operations to draw out initial DM, which records the probability of each pixel should be in-focused in each source image. Then we apply guided filter (He, Sun, and Tang 2013) to smooth the boundary of DM and acquire final DM. Finally, we cascade the fusion module in our structure and generate the fused result.

**Feature Extraction Path** As shown in Figure 1, the feature extraction path is a siamese architecture (Sergey and Nikos 2015), which uses the same architectures with the same weights. It consists of a cascade of four convolutional layers to extract multi-scale deep features from each source image, and use densely connection architecture to connect the output of each layer to the other layers, which strengthens feature propagation and reduces the number of parameters (Gao et al. 2017; Xu et al. 2020c). To precisely localize the details of the image, there are no pooling layers in our network.

In addition, we use squeeze and excitation (SE) module after each convolutional layer, which showed good performance at image recognition and segmentation (Jie, Li, and Gang 2018). It can effectively enhance spatial feature encoding by adaptive recalibrating channel-wise or spatial-feature responses. Same with (Ma et al. 2019), we use channel SE module (CSE) (Guha, Nassir, and Christian 2018) in feature extraction path. CSE uses a global average pooling layer to embed the global spatial information in a vector, which passes through two fully connected layers to acquire a new vector. This encodes the channel-wise dependencies, which can be used to recalibrate the original feature map in the channel direction.

After feature extraction, we calculate multi-scale activity levels using SF module (Ma et al. 2019). Consider two input images  $A$  and  $B$ , and a fused image  $F$ . Let  $DF$  be the deep features drawn from the convolutional layer of each scale.  $DF_{(m,n)}^A$  is one feature vector of pixel  $i$  in source image  $A$  with  $(m, n)$  coordinates. We calculate its SF by:

$$RF_{(m,n)}^A = \sqrt{\sum_{-r \leq a, b \leq r} [DF_{(m+a,n+b)}^A - DF_{(m+a,n+b-1)}^A]^2} \quad (1)$$

$$CF_{(m,n)}^A = \sqrt{\sum_{-r \leq a, b \leq r} [DF_{(m+a,n+b)}^A - DF_{(m+a-1,n+b)}^A]^2} \quad (2)$$

$$SF_{(m,n)}^A = \sqrt{\frac{(CF_{(m,n)}^A)^2 + (RF_{(m,n)}^A)^2}{(2r+1)^2}} \quad (3)$$

where  $RF$  and  $CF$  are respectively the row and column vector frequencies.  $r$  is the kernel radius and  $r = 5$  in our work. The original spatial frequency is block-based, while it is pixel-based in our method. We apply the same padding strategy at the borders of feature maps.

We subtract  $SF^B$  from  $SF^A$  to obtain activity level maps for each scale. Then we concatenate multi-scale activity level maps and feed them into the decision path.

**Decision Path** In decision path, we first use four convolutional layers to generate initial DM, which record the probability ( $p_i$ ) that each pixel ( $i$ ) of the source image  $A$  is more clear than that of the source image  $B$ . And the initial DM is optimized by loss function with ground truth DM, as shown in the next section.

In addition, we also use the SE module in the decision path. Specifically, we use spatial squeeze and channel excitation (SSE) (Guha, Nassir, and Christian 2018), to enhance the robustness and representatives of deep features. SSE uses a convolutional layer with one  $k_s \times k_s$  kernel to acquire a projection tensor ( $k_s = 7$  in our work). Each unit of the projection refers to the combined representation for all channels  $C$  at a spatial location and is used to spatially recalibrate the original feature map.

To smooth the boundary of the fused result, we utilize threshold operation to filter initial DM ( $p_i \notin [0.1, 0.8]$ ) and obtain the boundary region. And then we use guided filter (He, Sun, and Tang 2013) to obtain smooth DM. Finally, we use the boundary region as threshold region to combine smooth DM and initial DM to form final DM. That is the boundary of final DM is the smooth DM and the center of final DM is the initial DM. Note that we only use a threshold operation to generate boundary region and do not hinder the backpropagation of network, which means that our structure can be trained by an end-to-end training procedure. In addition, we do not use non-differentiable post-processing methods with empirical parameters, such as morphology operation and small region removal strategy. Then, we cascade a fusion module using the final DM and source images to generate the fused result. As shown in Eq 4, each pixel of fused image ( $F_i$ ) can be obtained by:

$$F_i = p_i \times Img_i^A + (1 - p_i) \times Img_i^B \quad (4)$$

where the probability ( $p_i$ ) in DM also means the fusion ratio of each pixel in the source images

Finally, we use gradient aware loss function to optimize the network to preserve gradient information in fused result.

In general, the network can simultaneously generate DM and fused result with end-to-end training procedure.

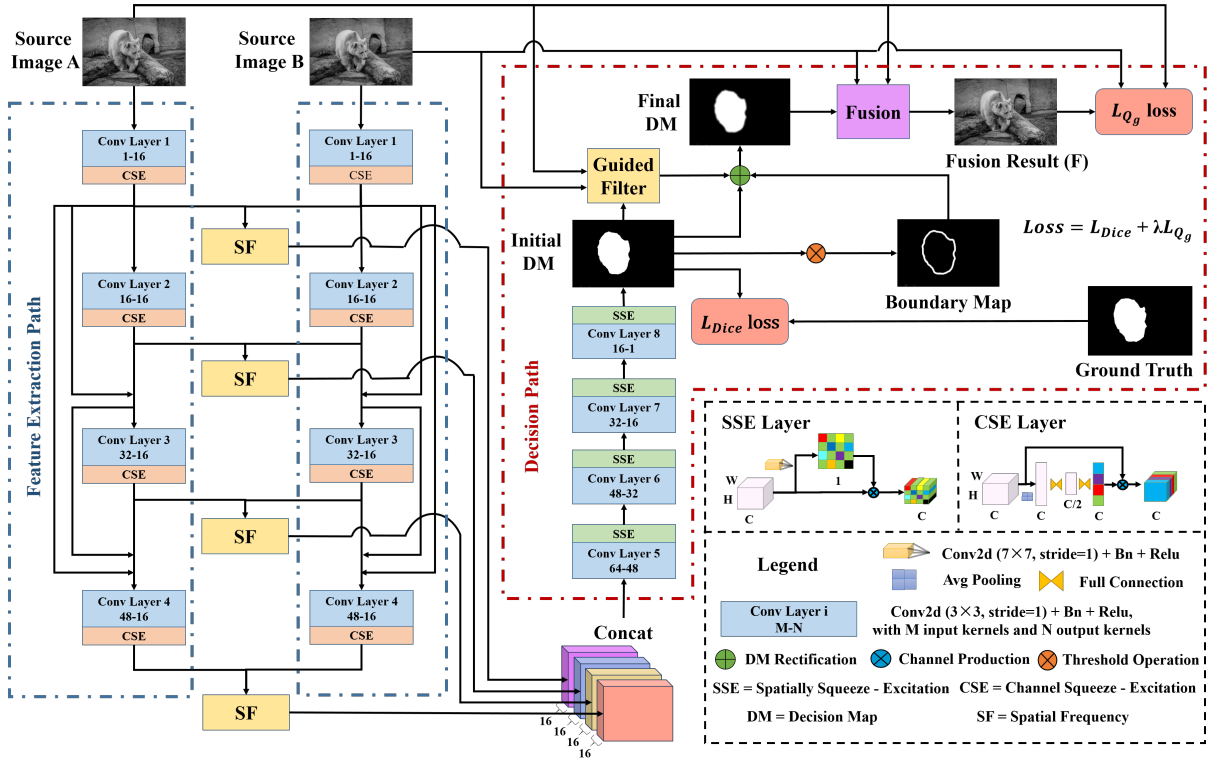


Figure 1: The network structure of the proposed algorithm.

## Loss Function

We define a gradient aware loss function to optimize the network to simultaneously output DM and clear fusing result. The final loss function is defined in Eq 5.

$$L = L_{Dice} + \lambda L_{Q_g} \quad (5)$$

where  $\lambda$  is a weight to balance the importance between two losses, and  $\lambda = 1$  in this work.

$L_{Dice}$  is a classical loss function in semantic segmentation (Fausto, Nassir, and Seyedahmad 2016), which is defined in Eq 6.

$$L_{Dice} = 1 - \frac{2 \sum_i^{N_P} p_i g_i + 1}{\sum_i^{N_P} p_i^2 + \sum_i^{N_P} g_i^2 + 1} \quad (6)$$

where the sums run over the  $N_P$  pixels, of the predicted binary segmentation map  $p_i \in DM$  and the ground truth map  $g_i \in G$ . Adding 1 is to mitigate the gradient vanishing issue.

In addition, we propose to use  $L_{Q_g}$  to optimize the network to export the final clear fused result. In the field of multi-focus image fusion, it is commonly speculated that only objects within the DOF have a sharp appearance in a photograph, while others are likely to be blurred (Liu et al. 2017). However, lots of previous works did not consider to preserve gradient information in network training. In this work, we focus on a classical gradient based fusion evaluation metric,  $Q_g$  or  $Q_F^{AB}$  (Xydeas and Petrovic 2000), and make it differentiable as loss function in an end-to-end training procedure. By using this optimization, we lead the net-

work to preserve gradient information in the final fused result.

$Q_g$  is an evaluation metric that measures the amount of edge information transferred from input images to the fused image (Xydeas and Petrovic 2000). Consider two input images  $A$  and  $B$ , and a fused image  $F$ . A sobel edge operator is applied to yield the edge strength  $g_i$  and orientation  $\alpha_i$  of each pixel  $i$ . Thus, for an input image  $A$ :

$$g_i^A = \sqrt{(s_i^{Ax})^2 + (s_i^{Ay})^2} \quad (7)$$

$$\alpha_i^A = \tan^{-1} \left( \frac{(s_i^{Ay})^2}{(s_i^{Ax})^2} \right) \quad (8)$$

where  $s_i^{Ax}$  and  $s_i^{Ay}$  are the respective convoluted results with the horizontal and vertical sobel templates.

The relative strength  $G_i^{AF}$  and orientation value  $\Delta_i^{AF}$  between input image  $A$  and fused image  $F$  are defined as:

$$G_i^{AF} = \begin{cases} \frac{g_i^F}{g_i^A}, & \text{if } g_i^A > g_i^F \\ \frac{g_i^A}{g_i^F}, & \text{if } g_i^A \leq g_i^F \end{cases} \quad (9)$$

$$\Delta_i^{AF} = 1 - \frac{|\alpha_i^A - \alpha_i^F|}{\pi/2} \quad (10)$$

Unfortunately, the Heaviside function in Eq 9 and absolute function in Eq 10 are not differentiable and thus cannot be included in training stage. Therefore, we propose to use



sigmoid function as a smooth approximation to the Heaviside function which is defined as:

$$f(x, y) = \frac{1}{1 + e^{-k(x-y)}}. \quad (11)$$

where  $k$  controls the steepness of the curve and closeness to the original Heaviside function, larger  $k$  means closer approximation ( $k = 1000$  in our work). Then, Eq 9 can be rewritten as Eq 12.

$$G_i^{AF} \approx f(g_i^F, g_i^A) \times \frac{g_i^A}{g_i^F} + (1 - f(g_i^F, g_i^A)) \times \frac{g_i^F}{g_i^A} \quad (12)$$

And Eq 10 can be rewritten as Eq 13.

$$\Delta_i^{AF} \approx 1 - \frac{(\alpha_i^A - \alpha_i^F) \times (2f(\alpha_i^A, \alpha_i^F) - 1)}{\pi/2} \quad (13)$$

Note that in pytorch implementation (Adam et al. 2019), the gradient of absolute function is 0 when input of that equals 0, which is differentiable. Thus it can use Eq 10 rather than Eq 13 in pytorch. The detailed analysis can be found in the experiment section.

The edge strength and orientation preservation values, respectively, can be derived as:

$$Q_{g_i}^{AF} = \frac{\Gamma_g}{1 + e^{k_g(G_i^{AF} - \sigma_g)}} \quad (14)$$

$$Q_{\alpha_i}^{AF} = \frac{\Gamma_\alpha}{1 + e^{k_\alpha(\Delta_i^{AF} - \sigma_\alpha)}} \quad (15)$$

where the constants  $\Gamma_g, k_g, \sigma_g$  and  $\Gamma_\alpha, k_\alpha, \sigma_\alpha$  determine the shapes of the respective sigmoid functions (same with Eq 11) used to form the edge strength and orientation preservation value. Normally,  $\Gamma_g = \Gamma_\alpha = 1, k_g = -10, k_\alpha = -20, \sigma_g = 0.5, \sigma_\alpha = 0.75$ . The edge information preservation value is then defined as:

$$Q_i^{AF} = Q_{g_i}^{AF} \times Q_{\alpha_i}^{AF} \quad (16)$$

The final assessment is obtained from the weighted average of the edge information preservation values:

$$L_{Q_g} = 1 - Q_g = 1 - \frac{\sum_i^{N_P} (Q_i^{AF} w_i^A + Q_i^{BF} w_i^B)}{\sum_i^{N_P} (w_i^A + w_i^B)} \quad (17)$$

where  $w_i^A = [g_i^A]^\gamma$  and  $w_i^B = [g_i^B]^\gamma$ .  $\gamma$  is a constant, and usually sets  $\gamma = 1$ .

In total, we modify a gradient based classical fusion evaluation metric ( $Q_g$ ) as a loss function to optimize the network to export clearly fused result.

### Decision calibration for multiple image fusion

The most applications of multi-focus fusion are based on multiple images. However, almost multi-focus fusion structures concentrated on two images scene and only used one by one serial fusion strategy for multiple image fusion. As shown in the top of Figure 2, one-by-one serial strategy needs to run  $2 \times (N_I - 1)$  times feature extraction paths and

$N_I - 1$  times decision paths, where  $N_I$  is the number of the source images. In this work, we propose a decision calibration strategy, which shown in the bottom of Figure 2. It only needs to run  $N_I$  times feature extraction paths and  $N_I - 1$  times decision paths by using the calibration module, which can generally decrease time consumption.

In decision calibration strategy, the first image is used as baseline, and feeds it to the structure with other images. Thus, we can save the parameters of the first image in the feature extraction path and avoid repeating computation. Then it uses final DMs drawn from each decision path to calculate the decision volume (DV), which records the activity levels of all the source images, as shown below equation.

$$DV_i^j = \begin{cases} p_i^2, & \text{if } j = 1 \\ 1 - p_i^2, & \text{if } j = 2 \\ \frac{p_i^2 \times (1 - p_i^j)}{p_i^j}, & \text{others} \end{cases} \quad (18)$$

where  $j \in \{1, \dots, N_I\}$ , is the index of the source image and  $p_i^j$  is the value of pixel  $i$  in final DM when fuses the source image 1 and the source image  $j$ .

Then, we choose the index of maximum in  $DV_i^j$  for each pixel  $i$  as the index of the most clarity pixel  $i$  in the source images. According to the above indices, we can obtain the entire resulting fused image.

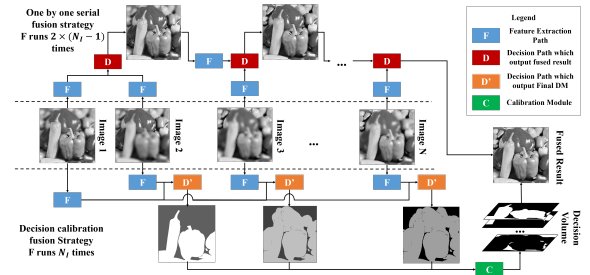


Figure 2: The flowchart of the traditional one-by-one serial fusion strategy (Top) and the proposed decision calibration strategy (Bottom).

## Experiment

### Dataset

**Training set** In the field of multi-focus image fusion, it is intractable to get the ground-truth fusion result of the real-world multi-focus images. Thus, we generate multi-focus image data based on MS COCO dataset (Lin et al. 2014). Specifically, we use the annotation of image segmentation as a threshold region to decide which part of the original image should be filtered by gaussian blurring. A visualization of training data can be found at supplementary material. Finally, we obtain 5786 multi-focus image pairs and their mask ground-truth and divide these into training and validation sets according to the ratio of 7:3.

**Testing set** We use 26 image pairs of publicly available multi-focus images from (Nejati, Samavi, and Shirani 2015; Savić and Babić 2012) as testing set for evaluation.

## Training Procedure

During training, all images were transformed to gray-scale and resized to  $256 \times 256$ , then random cropped to  $156 \times 156$ . Note that images were gray-scale in the training phase, while images for testing can be gray-scale or color images with RGB channels. For color images that needed to be fused, we transformed the images to gray-scale and calculated a decision map to fuse them. In addition to random crop, we also used some data augmentation methods, such as random blur, random offset, gaussian noise, which will be discussed in detail later. The initial learning rate was  $1 \times 10^{-4}$ , and this was decreased by a factor of 0.8 at every two epochs. We optimized the objective function by Adam (Kingma and Ba 2015). The batch size and number of epochs were 16 and 50, respectively. Our implementation was derived from the publicly available Pytorch framework (Adam et al. 2019). The network’s training and testing were performed on a station using a NVIDIA Tesla V100 GPU with 32 GB memory.

## Evaluation Metrics

We use six classical fusion metrics:  $Q_g$  (Xydeas and Petrovic 2000),  $Q_y$  (Yang et al. 2008),  $Q_{ncie}$  (Qiang, Yi, and Jing 2008),  $Q_{cb}$  (Chen and Blum 2009),  $FMI\_EDGE$  and  $FMI\_DCT$  (Haghighat, Aghagolzadeh, and Seyedarabi 2011) to evaluate the quality of fused result. A larger value of any of the above six metrics indicates better fusion performance. The detailed definition of these metrics can be found at supplementary material. For fair comparison, we use appropriate default parameters for these metrics, and all codes are derived from their public resources (Liu 2012; Mohammad and Amirkabiri 2014).

## Comparison

To demonstrate the performance of our method, we compare it with recent SOTA fusion methods in objective and subjective assessments. Five deep learning based methods with two of them are DM based methods (CNN-Fuse (Liu et al. 2017) and SESF-Fuse (Ma et al. 2019)), and three of them are decoder based methods (DenseFuse (Li and Wu 2019), IFCNN (Zhang et al. 2020b) and PMGI (Zhang et al. 2020a)). In addition, for CNN-Fuse and SESF-Fuse, we also compare different versions of whether to use post-processing (pp) methods (or consistency verification) with empirical parameters.

In addition, in supplementary material, we also present the comparison of fusion quality and runtime with traditional fusion algorithms, such as dense SIFT (DSIFT) (Liu, Liu, and Wang 2015), multi-scale weighted gradient (MWG) (Zhou, Li, and Wang 2014), focus-stack (Andrew 2013), sparse representation (SR) (Yang and Li 2010), non-subsampled contourlet transform (NSCT) (Zhang and long Guo 2009), curvelet transform (CVT) (Nencini et al. 2007), dual-tree complex wavelet transform (DTCWT) (Lewis et al. 2007), spatial frequency (SF) (Li, Kwok, and Wang 2001), discrete wavelet transform (DWT) (Li, Manjunath, and Mitra 1995), ratio of low-pass pyramid (RP) (Toet 1989), and laplacian pyramid (LP) (Burt and Adelson 1983). And our method generally achieves better performance compared to traditional algorithms.

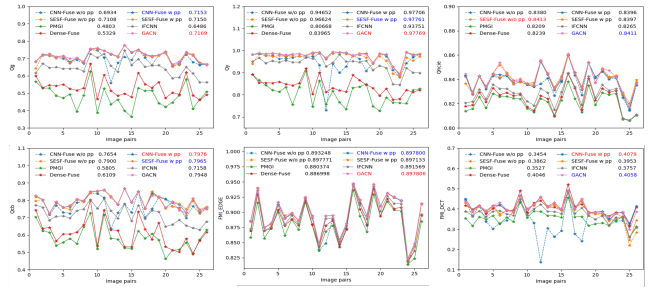


Figure 3: Objective Assessments of our GACN with other SOTA algorithms. Means of metrics for different algorithms are shown in the legends, and evaluation for each image pair is shown in the plot. Optimal values are shown in red and sub-optimal values in blue.

**Objective Assessment** We illustrate the assessment plot of the above six metrics with different fusion algorithms in Figure 3. DM based algorithms generate an intermediate decision map to decide which pixel should appear in the fused result, which can precisely preserve true pixel values of the source image. And decoder based algorithms directly use a decoder to draw out the fused result and cannot preserve true pixel values because of the nonlinear mapping mechanism in the decoder. Therefore, DM based algorithms achieve high performance in objective assessments, while decoder based algorithms show poor performance. In addition, DM based algorithms rely on post-processing methods to rectify DM, so the performance will degrade if we remove it. Our algorithm, GACN can simultaneously generate decision map and fused result with end-to-end training procedure, and gradient information can be preserved by the gradient loss function. Our method achieves the promising performance compared to SOTA algorithms with no post-processing methods with empirical parameters.

**Subjective Assessment** We show three samples with different fusion methods in Figure 4, such as 'seaboard', 'horse', and 'stone lion'. CNN-Fuse and SESF-Fuse achieve better fusion performance, however, they rely on post-processing methods with empirical parameters, such as morphology operation and small size removal strategy. If we remove these methods, there will be some artifacts that appear on the results, such as an unnatural transition in 'seaboard' and 'stone lion' results and blob noisy in the sky on 'seaboard' for SESF-Fuse without post-processing. Besides, the threshold of region removal strategy is an empirical parameter which hard to adjust. For the small region between halter and horse mouth in the 'horse' image is actually a background region, but the region removal strategy will incorrectly remove it so that the results of CNN-Fuse and SESF-Fuse with post-processing will export blurring results. While it shows clearly fused result without post-processing. In a word, post-processing with empirical parameters is hard to adjust according to the application scene. In addition, decoder based methods cannot precisely preserve the true pixel values. For example, there is some color distortion in fused results of PMGI. And the fused result of DenseFuse is more blurred than other methods. IFCNN cannot handle small dis-

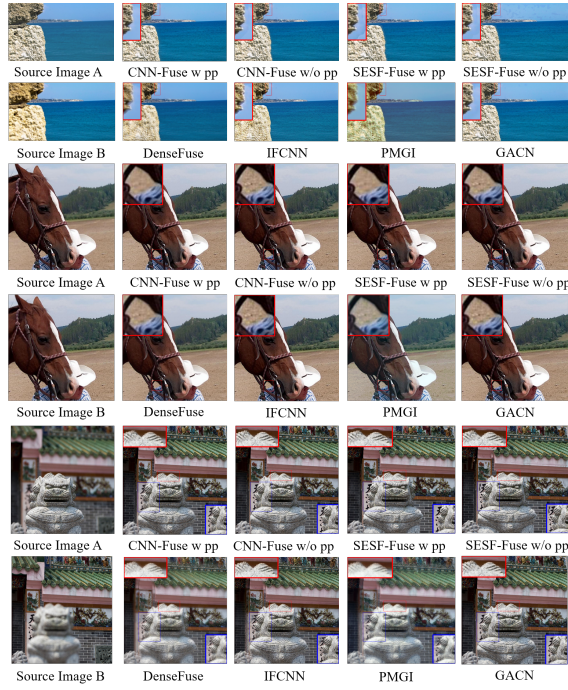


Figure 4: Visualization of three examples with different fusion algorithm. For each example, Source Image A is foreground focused and Source Image B is background focused. Some annotated rectangles and their magnified results are shown in the fused results.

placement in source images because it doesn't smooth the boundary region, as shown in 'stone lion' results. And fortunately, Our method, GACN, achieves robust promising fusing performance at all examples.

### Ablation Study

We evaluate our method with different settings to verify the contribution of each module.

**Loss Function Study** To verify the contribution of loss functions, we present an experiment of different loss settings in the supplementary material. We compare the performance of different combinations of mask-based and gradient-based loss functions. The mask based loss functions include  $L_{Dice}$  (Fausto, Nassir, and Seyedahmad 2016),  $L_{Focal}$  (Tsung-Yi et al. 2017), and  $L_{BCE}$  (Saining and Zhuowen 2015). While gradient-based loss functions include  $L_{Q_g}$ ,  $L_{EG}$  (Li et al. 2020), and  $L_{ST}$  (H et al. 2020). Where  $EG$  refers to edge-preserving loss and  $ST$  means structure tensor loss. According to the experiment, we note that the performance of the combination of  $L_{Dice}$  and  $L_{Q_g}$  outperforms other loss settings in most the metrics, which means that the above two losses will both lead the network to export promising fused result.

**Differentiation Study** In pytorch, the absolute function of angle calculation in Eq 10 is differentiable, and it is no need to use smooth approximation Eq 13. However, it might not

be universal for other frameworks, thus we compare the performance of the above settings in the supplementary material. We found that directly using the absolute function is a little better than a smooth approximation, which might be the reason for gradient vanish in the sigmoid calculation.

**Augmentation Study** We conduct an experiment to exploit the impact of augmentation methods in the supplementary material. We pick some different augmentation methods, such as random gaussian noise, random offset, and random blurring. We find they all show an increase in the evaluation and it achieves the best performance when we combine above all augmentation methods.

**SE Modules Study** We illustrate an experiment to exploit the impact of different SE modules on the decision path in the supplementary material. We compare three variant SE modules proposed by (Guha, Nassir, and Christian 2018), such as SSE, CSE, and concurrent CSE and SSE (SCSE). According to the experiment, we find that SSE achieves the best performance, which means that spatial recalibration is more important and robust than channel recalibration in the decision path for gradient calculation.

### Multiple image fusion with multi-focus

We show two examples of multiple image fusion in Figure 5. The 'strawberry' is acquired from (Xu et al. 2020d). And the microscopic image 'chip' (with size of  $2700 \times 1800$ ) is obtained by a microscope that takes pictures with lots of different focus points. According to previous statement and experiment in supplementary material, decision calibration for 'chip' images fusion can actually increase execution efficiency by about 30.65% compared to one-by-one serial strategy (0.7138's to 0.4950's for each image), which is more feasible for industrial application. More detailed analysis can be found in the supplementary material.

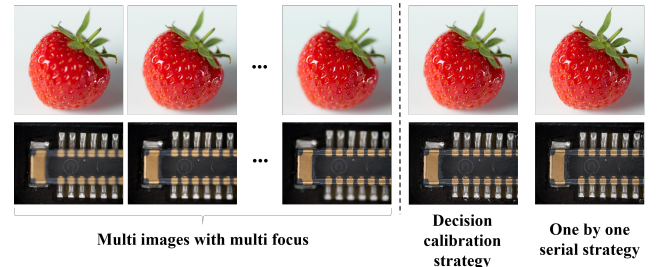


Figure 5: Visualization of multiple image fusion.

### Conclusion

In this work, we propose a network to simultaneously generate decision map and fused result with an end-to-end training procedure. It avoids utilizing empirical post-processing methods in the inference stage. Besides we introduce a gradient aware loss function to lead the network to preserve gradient information. Also we design a decision calibration strategy to fuse multiple images, which can increase implementation efficiency. Extensive experiments are conducted

to compare with existing SOTA multi-focus image fusion structures, which shows that our designed structure can generally ameliorate the output fused image quality for multi-focus images, and increase implementation efficiency over 30% for multiple image fusion. We will further improve the fusion performance of multiple image fusion in future work.

## Acknowledgments

We acknowledge the support of the National Key Research and Development Program of China (No. 2016YFB0700500). The computing work is supported by USTB MatCom of Beijing Advanced Innovation Center for Materials Genome Engineering. Besides, the dataset of multiple image fusion is driven from the website provided by Zhuhai Boming Vision Technology Co., Ltd.

## References

- Adam, P.; Sam, G.; Francisco, M.; Adam, L.; James, B.; Gregory, C.; Trevor, K.; Zeming, L.; Natalia, G.; and Luca, A. 2019. Pytorch: An imperative style, high-performance deep learning library. In *Advances in neural information processing systems*, 8026–8037.
- Andrew, C. 2013. Focus Stacking Made Easy with Photoshop. <https://github.com/cmcguinness/focusstack>.
- Burt, P.; and Adelson, E. 1983. The Laplacian Pyramid as a Compact Image Code. *IEEE Transactions on Communications* 31(4): 532–540. ISSN 0090-6778. doi:10.1109/TCOM.1983.1095851.
- Chen, Y.; and Blum, R. S. 2009. A new automated quality assessment algorithm for image fusion. *Image and Vision Computing* 27(10): 1421 – 1432. ISSN 0262-8856. doi: <https://doi.org/10.1016/j.imavis.2007.12.002>.
- Fausto, M.; Nassir, N.; and Seyedahmad, A. 2016. V-Net: Fully Convolutional Neural Networks for Volumetric Medical Image Segmentation. In *International Conference on 3D Vision*, 565–571.
- Gao, H.; Zhuang, L.; Laurens, V. D. M.; and Q, W. K. 2017. Densely connected convolutional networks. In *Proceedings of the IEEE conference on computer vision and pattern recognition*, 4700–4708.
- Guha, R. A.; Nassir, N.; and Christian, W. 2018. Concurrent spatial and channel squeeze and excitation in fully convolutional networks. In *International Conference on Medical Image Computing and Computer-Assisted Intervention*, 421–429. Springer.
- H, J.; Y, K.; H, J.; N, H.; and Sohn. 2020. Unsupervised Deep Image Fusion With Structure Tensor Representations. *IEEE Transactions on Image Processing* 29: 3845–3858.
- Haghighat, M. B. A.; Aghagolzadeh, A.; and Seyedarabi, H. 2011. A non-reference image fusion metric based on mutual information of image features. *Computers and Electrical Engineering* 37(5): 744 – 756. ISSN 0045-7906. doi: <https://doi.org/10.1016/j.compeleceng.2011.07.012>.
- He, K.; Sun, J.; and Tang, X. 2013. Guided Image Filtering. *IEEE Transactions on Pattern Analysis and Machine Intelligence* 35(6): 1397–1409. ISSN 0162-8828. doi: 10.1109/TPAMI.2012.213.
- Huang, J. H.; Le, Z.; Ma, Y. T.; Mei, X.; and Fan, F. 2020. A generative adversarial network with adaptive constraints for multi-focus image fusion. *Neural Computing and Applications* 1–11.
- Jie, H.; Li, S.; and Gang, S. 2018. Squeeze-and-Excitation Networks. In *The IEEE Conference on Computer Vision and Pattern Recognition (CVPR)*.
- Kingma, D. P.; and Ba, J. 2015. Adam: A Method for Stochastic Optimization. In *International Conference on Learning Representations*.
- Lewis, J. J.; Callaghan, R. J. O.; Nikolov, S. G.; Bull, D. R.; and Canagarajah, N. 2007. Pixel- and region-based image fusion with complex wavelets. *Information Fusion* 8(2): 119 – 130. ISSN 1566-2535. doi: <https://doi.org/10.1016/j.inffus.2005.09.006>.
- Li, H.; Manjunath, B.; and Mitra, S. 1995. Multisensor Image Fusion Using the Wavelet Transform. *Graphical Models and Image Processing* 57(3): 235 – 245. ISSN 1077-3169. doi: <https://doi.org/10.1006/gmip.1995.1022>.
- Li, H.; and Wu, X. 2019. DenseFuse: A Fusion Approach to Infrared and Visible Images. *IEEE Transactions on Image Processing* 28: 2614–2623.
- Li, J.; Guo, X.; Lu, G.; Zhang, B.; Xu, Y.; Wu, F.; and Zhang, D. 2020. DRPL: Deep Regression Pair Learning for Multi-Focus Image Fusion. *IEEE Transactions on Image Processing* 29: 4816–4831.
- Li, S.; Kang, X.; Fang, L.; Hu, J.; and Yin, H. 2017. Pixel-level image fusion: A survey of the state of the art. *Information Fusion* 33: 100 – 112. ISSN 1566-2535. doi: <https://doi.org/10.1016/j.inffus.2016.05.004>.
- Li, S.; Kwok, J. T.; and Wang, Y. 2001. Combination of images with diverse focuses using the spatial frequency. *Information Fusion* 2(3): 169 – 176. ISSN 1566-2535. doi: [https://doi.org/10.1016/S1566-2535\(01\)00038-0](https://doi.org/10.1016/S1566-2535(01)00038-0).
- Lin, T.-Y.; Maire, M.; Belongie, S.; Hays, J.; Perona, P.; Ramanan, D.; Dollár, P.; and Zitnick, C. L. 2014. Microsoft coco: Common objects in context. In *European conference on computer vision*, 740–755. Springer.
- Liu, Y.; Chen, X.; Peng, H.; and Wang, Z. 2017. Multi-focus image fusion with a deep convolutional neural network. *Information Fusion* 36: 191 – 207. ISSN 1566-2535. doi: <https://doi.org/10.1016/j.inffus.2016.12.001>.
- Liu, Y.; Liu, S.; and Wang, Z. 2015. Multi-focus image fusion with dense SIFT. *Information Fusion* 23: 139 – 155. ISSN 1566-2535. doi: <https://doi.org/10.1016/j.inffus.2014.05.004>.
- Liu, Z. 2012. Image Fusion Metrics. <https://github.com/zhengliu6699/imageFusionMetrics>.
- Ma, B.; Zhu, Y.; Yin, X.; Ban, X.; and Huang, H. 2019. SESF-Fuse: An Unsupervised Deep Model for Multi-Focus Image Fusion. *arXiv*.



- Mohammad, H.; and Amirkabiri, R. M. 2014. Fast-FMI: non-reference image fusion metric. In *2014 IEEE 8th International Conference on Application of Information and Communication Technologies (AICT)*, 1–3. IEEE.
- Nejati, M.; Samavi, S.; and Shirani, S. 2015. Multi-focus image fusion using dictionary-based sparse representation. *Information Fusion* 25: 72 – 84. ISSN 1566-2535. doi: <https://doi.org/10.1016/j.inffus.2014.10.004>.
- Nencini, F.; Garzelli, A.; Baronti, S.; and Alparone, L. 2007. Remote sensing image fusion using the curvelet transform. *Information Fusion* 8(2): 143 – 156. ISSN 1566-2535. doi: <https://doi.org/10.1016/j.inffus.2006.02.001>.
- Qiang, W.; Yi, S.; and Jing, J. 2008. Performance evaluation of image fusion techniques. *Image fusion: algorithms and applications* 19: 469–492.
- Ram, P. K.; Sai, S. V.; and Venkatesh, B. R. 2017. DeepFuse: A Deep Unsupervised Approach for Exposure Fusion with Extreme Exposure Image Pairs. In *ICCV*, volume 1, 3.
- Saining, X.; and Zhuowen, T. 2015. Holistically-nested edge detection. In *Proceedings of the IEEE international conference on computer vision*, 1395–1403.
- Savić, S.; and Babić, Z. 2012. Multifocus image fusion based on empirical mode decomposition. In *19th IEEE International Conference on Systems, Signals and Image Processing (IWSSIP)*.
- Sergey, Z.; and Nikos, K. 2015. Learning to compare image patches via convolutional neural networks. In *Proceedings of the IEEE conference on computer vision and pattern recognition*, 4353–4361.
- Tang, H.; Xiao, B.; Li, W.; and Wang, G. 2017. Pixel Convolutional Neural Network for Multi-Focus Image Fusion. *Information Sciences* S0020025517311647. doi: <https://doi.org/10.1016/j.ins.2017.12.043>.
- Toet, A. 1989. Image fusion by a ratio of low-pass pyramid. *Pattern Recognition Letters* 9(4): 245 – 253. ISSN 0167-8655. doi: [https://doi.org/10.1016/0167-8655\(89\)90003-2](https://doi.org/10.1016/0167-8655(89)90003-2).
- Tsung-Yi, L.; Priya, G.; Ross, G.; Kaiming, H.; and Piotr, D. 2017. Focal loss for dense object detection. In *Proceedings of the IEEE international conference on computer vision*, 2980–2988.
- Xu, H.; Fan, F.; Zhang, H.; Le, Z.; and Huang, J. 2020a. A Deep Model for Multi-Focus Image Fusion Based on Gradients and Connected Regions. *IEEE Access* 8: 26316–26327.
- Xu, H.; Ma, J.; Jiang, J.; Guo, X.; and Ling, H. 2020b. U2Fusion: A Unified Unsupervised Image Fusion Network. *IEEE Transactions on Pattern Analysis and Machine Intelligence*.
- Xu, H.; Ma, J.; Le, Z.; Jiang, J.; and Guo, X. 2020c. FusionDN: A Unified Densely Connected Network for Image Fusion. In *AAAI*.
- Xu, S.; Wei, X.; Zhang, C.; Liu, J.; and Zhang, J. 2020d. MFFW: A new dataset for multi-focus image fusion. *arXiv preprint arXiv:2002.04780*.
- Xydeas, C. S.; and Petrovic, V. 2000. Objective image fusion performance measure. *Electronics Letters* 36(4): 308–309. ISSN 0013-5194. doi: [10.1049/el:20000267](https://doi.org/10.1049/el:20000267).
- Yang, B.; and Li. 2010. Multifocus Image Fusion and Restoration With Sparse Representation. *IEEE Transactions on Instrumentation and Measurement* 59(4): 884–892. ISSN 0018-9456. doi: [10.1109/TIM.2009.2026612](https://doi.org/10.1109/TIM.2009.2026612).
- Yang, C.; Zhang, J. Q.; Wang, X. R.; and Liu, X. 2008. A novel similarity based quality metric for image fusion. *Information Fusion* 9(2): 156–160.
- Yann, L.; Yoshua, B.; and Geoffrey, H. 2015. Deep learning. *Nature* 521(7553): 436–444.
- Zhang, H.; Le, Z.; Shao, Z.; Xu, H.; and Ma, J. 2021. MFF-GAN: An unsupervised generative adversarial network with adaptive and gradient joint constraints for multi-focus image fusion. *Information Fusion* 66: 40 – 53. ISSN 1566-2535. doi: <https://doi.org/10.1016/j.inffus.2020.08.022>.
- Zhang, H.; Xu, H.; Xiao, Y.; Guo, X.; and Ma, J. 2020a. Rethinking the Image Fusion: A Fast Unified Image Fusion Network based on Proportional Maintenance of Gradient and Intensity. In *AAAI*, 12797–12804.
- Zhang, Q.; and long Guo, B. 2009. Multifocus image fusion using the nonsubsampling contourlet transform. *Signal Processing* 89(7): 1334 – 1346. ISSN 0165-1684. doi: <https://doi.org/10.1016/j.sigpro.2009.01.012>.
- Zhang, Y.; Liu, Y.; Sun, P.; Yan, H.; Zhao, X.; and Zhang, L. 2020b. IFCNN: A general image fusion framework based on convolutional neural network. *Information Fusion* 54: 99–118.
- Zhou, Z.; Li, S.; and Wang, B. 2014. Multi-scale weighted gradient-based fusion for multi-focus images. *Information Fusion* 20: 60 – 72. ISSN 1566-2535. doi: <https://doi.org/10.1016/j.inffus.2013.11.005>.